Research Square

Preprints are preliminary reports that have not undergone peer review.
They should not be considered conclusive, used to inform clinical practice,
or referenced by the media as validated information.

Siloxane-Containing Vinyl Ester Coatings for Cellulose-Based Substrates: Balancing Thermal, Saltwater-Barrier, and Mechanical Properties

Mengde Wu

151958055680163.com

State Key Laboratory of Chemistry for NBC Hazards Protection

Ge Cao

Guangdong Polytechnic

Yi Yu

State Key Laboratory of Chemistry for NBC Hazards Protection

Research Article

Keywords: Siloxane-modified vinyl ester resin, Multifunctional composite coatings, Thermal resistance, Saltwater resistance, Mechanical properties

Posted Date: November 13th, 2026

DOI: https://doi.org/10.21203/rs.3.rs-11520814/v1

License: This work is licensed under a Creative Commons Attribution 4.0 International License.
Read Full License

Additional Declarations: No competing interests reported.

Siloxane-Containing Vinyl Ester Coatings for Cellulose-Based Substrates: Balancing Thermal, Saltwater-Barrier, and Mechanical Properties

Mengde Wu [a*], Ge Cao [b,c*], Yi Yu [a]

[a] State Key Laboratory of Chemistry for NBC Hazards Protection, Beijing 102205, China

[b] Institute of Corrosion Science and Technology, Guangzhou 510530, China

[c] School of Textiles, Guangdong Polytechnic, Foshan, 528041, China

Corresponding authors: Mengde Wu (15195805568@163.com); Ge Cao (gcao@icost.ac.cn).

Acknowledgments

This work was supported by the Graduate Research and Innovation Projects of Jiangsu Province (No. KYCX23_0449), the National Key Research and Development Program of China (No. 2021YFB3701700), and the National Natural Science Foundation of China (No. 52603081).

Abstract: Developing multifunctional coatings that simultaneously provide thermal protection, moisture resistance, and mechanical integrity remains challenging for cellulose-based materials. Herein, siloxane-modified vinyl ester resin (SMER) composite coatings incorporating thermally stable inorganic fillers were developed for cellulose-based templates (CBTs). The effects of SMER content (10–40 wt%) on coating structure and protective performance were systematically investigated. Spectroscopic and microscopic analyses revealed the incorporation of silicon-containing components and composition-dependent morphological heterogeneity. Increasing SMER content enhanced the char yield at 700 °C from 35.91% to 53.46% and raised the final decomposition temperature from 600 to 642 °C. The 30 and 40 wt% coatings exhibited hydrophobic surfaces with water contact angles exceeding 90°. After immersion in 3.5 wt% NaCl solution for 3 days, the 40 wt% coating reduced saltwater absorption to 7.66%, compared with 38.65% for uncoated CBTs. Notably, the 10 wt% coating exhibited the longest heat-resistance time of 327.4 s at 250 °C, whereas the 30 wt% coating achieved the highest engineering stress at break (6.69 MPa) and elongation at break (82.06%). These findings reveal distinct composition-dependent trade-offs among thermal response, moisture resistance, and mechanical performance, providing insights into the rational design of multifunctional protective coatings for cellulose-based materials.

Keywords: Siloxane-modified vinyl ester resin; Multifunctional composite coatings; Thermal resistance; Saltwater resistance; Mechanical properties

Abbreviations

VE: Vinyl ester

SMER: Siloxane-modified vinyl ester resin

WCA: Water contact angle

CBT: Cellulose-based template

PDMS: Poly(dimethylsiloxane)

MEKP: Methyl ethyl ketone peroxide

SEM: Scanning electron microscopy

FT-IR: Fourier transform infrared spectroscopy

EDS: Energy-dispersive X-ray spectroscopy

XPS: X-ray photoelectron spectroscopy

TGA: Thermogravimetric analysis

DTG: Derivative thermogravimetry

IDT: Initial decomposition temperature

FDT: Final decomposition temperature

DSC: Differential scanning calorimetry

1. Introduction

Vinyl ester (VE) resins have attracted considerable attention as versatile thermosetting materials owing to their excellent chemical resistance, mechanical robustness, and rapid curing characteristics [1–4]. These advantages have enabled their widespread application in structural adhesives, protective coatings, and fiber-reinforced composites for automotive, aerospace, and marine engineering [5–9]. Nevertheless, their thermal response, environmental durability, and mechanical performance are strongly influenced by resin formulation, curing behavior, and network structure [10–15]. These limitations are particularly relevant to cellulose-based

combustible cartridge cases (CCCs), which require protective coatings capable of withstanding thermal exposure and moisture- and salt-containing environments while maintaining structural integrity. Various strategies have been explored to enhance VE performance, including nanocarbon reinforcement and flame-retardant modification. For instance, Yang et al. [16] reported improvements of 45% and 54% in the intrinsic stress-intensity factor and strain-energy release rate, respectively, while Zhang et al. [17] developed a flame-retardant VE formulation with a limiting oxygen index of 38.3%. Zhao et al. [18] employed a cross-linking strategy to modify VE, reducing its peak total smoke release rate by up to 67.8%. Despite these advances, achieving balanced thermal, environmental, and mechanical performance within a single coating system remains challenging.

Siloxane-containing polymers, particularly polydimethylsiloxane (PDMS), have emerged as promising modifiers because of their low surface energy, molecular flexibility, and water-repellent characteristics [19,20]. Their Si–O–Si backbone also provides favorable chemical and thermal characteristics, making them attractive components for organic–inorganic hybrid materials [21–26]. Incorporating siloxane components into VE-based matrices offers a potential strategy to combine the mechanical characteristics of thermosetting resins with improved surface hydrophobicity and environmental resistance. Furthermore, introducing thermally stable inorganic fillers may contribute to improved thermal performance. However, the overall properties of such multicomponent composites depend strongly on component compatibility, filler dispersion, coating morphology, and network characteristics. Excessive modifier incorporation may introduce structural heterogeneity and defects, potentially compromising mechanical integrity despite improvements in other protective functions. Therefore, understanding composition-dependent performance trade-offs is essential for optimizing multifunctional VE-based composite coatings.

Previous studies on protective coatings for CCCs and related cellulose-based structures have primarily focused on thermal resistance, moisture protection, salt-environment durability, or mechanical reinforcement [27–31]. Related protective technologies have also been investigated for cables, building components, and structural composites [32–35], while cellulose-derived materials have been explored for other functional protection applications [36]. However, differences in substrate characteristics and service requirements limit the direct

applicability of these findings to cellulose-based CCCs. More importantly, systematic investigations into the relationships among coating composition, chemical characteristics, microstructure, and multifunctional protective performance (water repellency, heat resistance, and saltwater-barrier properties) remain insufficient for siloxane-modified VE systems. In particular, whether increasing modifier content can simultaneously improve thermal durability, saline-water resistance, and mechanical properties, or instead produces competing performance trends, requires systematic investigation.

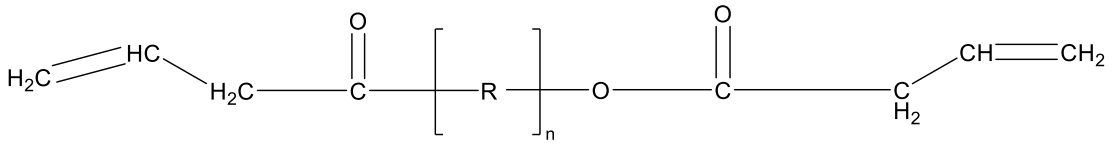
Herein, siloxane-modified vinyl ester resin (SMER) composite coatings with different SMER contents (10–40 wt%) were developed for protecting cellulose-based substrates. The coatings integrate a VE-based matrix, siloxane-containing components, and thermally stable inorganic fillers to provide complementary protective functions. Their chemical characteristics, morphology, thermal behavior, surface wettability, saline-water resistance, and tensile properties were systematically investigated. The results reveal distinct composition-dependent trends: intermediate SMER content provides the highest tensile performance, whereas higher SMER content favors saline-water resistance and high-temperature residue retention. Meanwhile, heat-exposure resistance exhibits a non-monotonic dependence on composition and test temperature. These findings highlight the importance of balancing multiple protective properties through formulation optimization and provide insights into the design of multifunctional thermosetting composite coatings for cellulose-based engineering applications.

2. Materials and methods

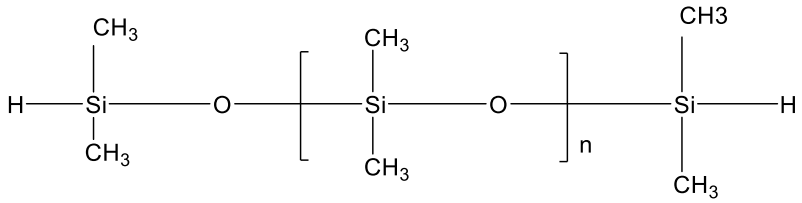
2.1 Materials

The resin examined in this work consisted of a bisphenol-A epoxy-based VE resin (ATLAC 580 ACT, DSM Composite Resins). Fig. 1a illustrates the chemical composition of the vinyl ester resin. The mean number of bisphenol-A units (n) in the dimethacrylate backbone was approximately 0.56, and the vinyl-ester monomer contained two vinyl terminal groups that formed a cross-linked structure throughout the polymerization process. Methyl ethyl ketone peroxide (MEKP, AR, $C_8H_{18}O_6$, molecular weight: 210.22 g/mol) was supplied by the Huntsman Chemical Company, Australia. Yttria-stabilized zirconia (CP, 99.0%, 50 nm) was sourced from Shanghai Yaoyi Alloy Material Co., Ltd., and the 593 epoxy resin curing agent (GR, 99.0%) was obtained from

Suzhou Qicai Stone Composite Material Co., Ltd. Si_3N_4 powder (KM-20 μm) was acquired from Suzhou Kangmai New Material Co., Ltd. In addition, sepiolite powder (400 mesh) was supplied by Macklin, and OP-4 emulsifier (alkylphenol polyoxyethylene ether, GR) and Tween 80 (polysorbate 80, AR) were supplied by Nanjing Middle East Glass Instrument Co., Ltd. Karstedt's catalyst consisted of a platinum(0)-1,3-divinyl-1,1,3,3-tetramethyldisiloxane complex solution in xylene with about 2% Pt metal, purchased from Macklin. PDMS (AR, 0.977 g/mL, 99.0%, end group: hydride-terminated PDMS, molecular weight: 5000 g/mol, viscosity: 5000 cP) was purchased from Aladdin. Fig. 1b presents the molecular configuration of the PDMS.



(a)



(b)

Fig. 1 Chemical structure of (a) vinyl ester resin and (b) PDMS

2.2 Preparation of the composite coating mixture

2.2.1 Synthesis of the SMER

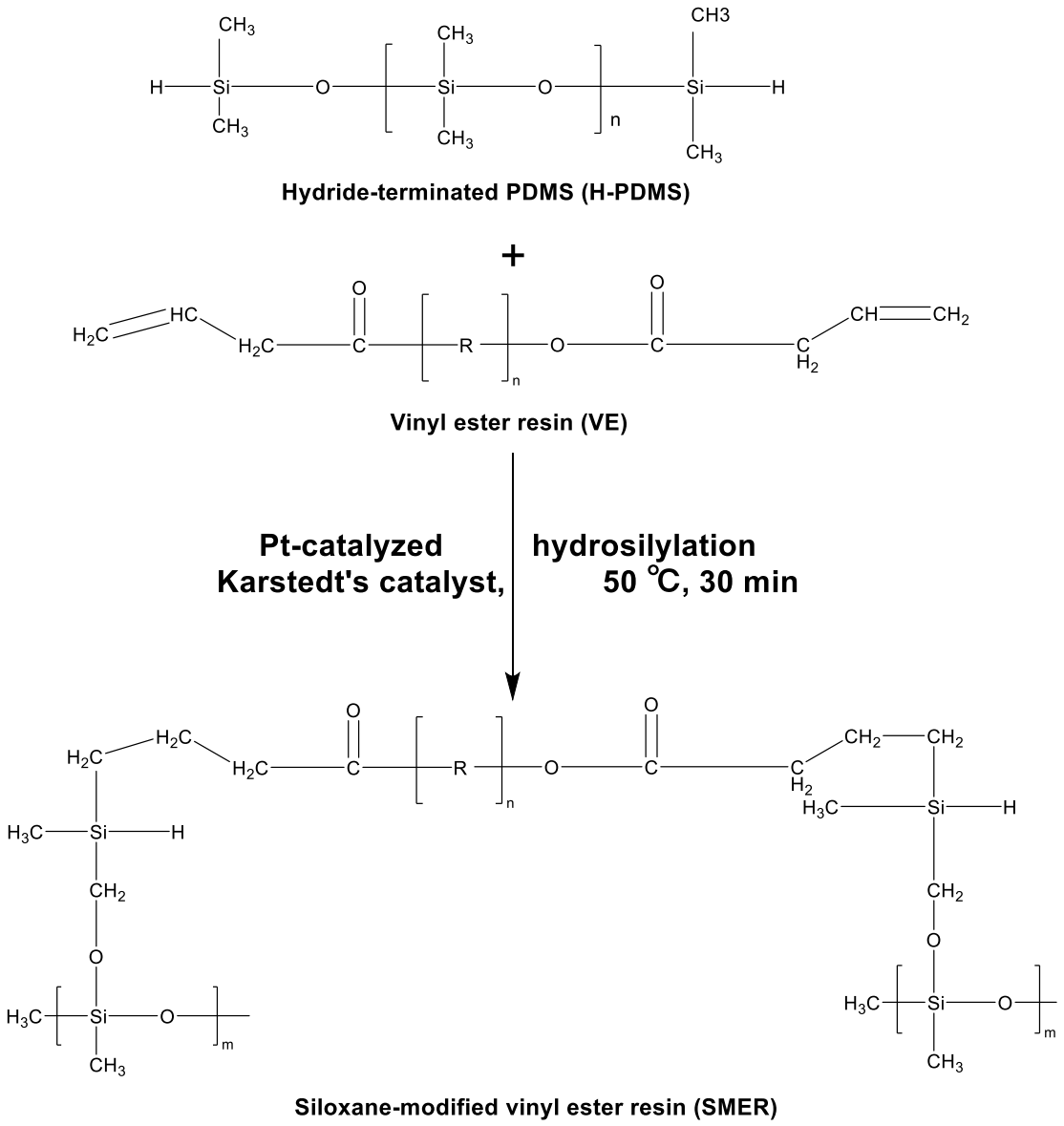


Fig. 2 Synthesis route of the siloxane-modified vinyl ester resin

Karstedt's catalyst is a homogeneous platinum catalyst widely used to promote hydrosilylation between Si-H and vinyl groups [37-41]. In such systems, activation of Si-H enables addition across C=C bonds and formation of Si-C linkages under relatively mild conditions.

The SMER was obtained by a copolymerized grafting reaction, as shown in Fig. 2, mainly from the vinyl ester resin and PDMS resin with different feed ratios (details are shown in Table 1). Subsequently, 0.2 g (approximately 0.2 mL) of Karstedt's catalyst solution was added into the above mixed solution and then stirred at 50 °C for 30 min. The Si_3N_4 and sepiolite powders were added in turn to the above mixture within 20 min. In addition, yttria-stabilized zirconia was introduced into the blend and continuously stirred at 60 °C for 10 min. OP-4 emulsifier and Tween 80 were also introduced into the blend under stirring at 70 °C for 1 h to obtain an even mixture solution (as shown in Fig. 3a).

2.2.2 Fabrication of the SMER composite coating solutions

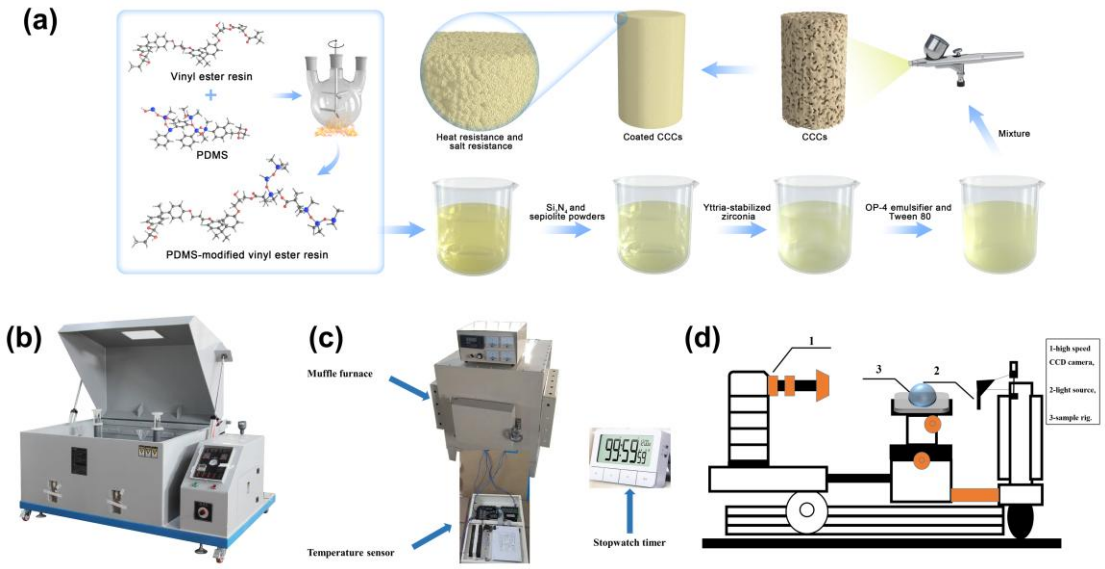


Fig. 3 Fabrication process of the SMER composite coating

Table 1 Formula of SMER composite coatings

Composite coatings	SMER (g)	Si_3N_4 (g)	Sepiolite powders (g)	Yttria-stabilized zirconia (g)	OP-4 emulsifier (g)	Tween 80 (g)	MEKP (g)	593 epoxy resin curing agents (g)
10 wt% SMER	2.2	1.0	3.0	2.5	1.5	2.0	5.0	5.0
20 wt% SMER	5.0	1.0	3.0	2.5	1.5	2.0	5.0	5.0
30 wt% SMER	8.6	1.0	3.0	2.5	1.5	2.0	5.0	5.0
40 wt% SMER	13.3	1.0	3.0	2.5	1.5	2.0	5.0	5.0

Annotation: SMER content computational formula:

$$XX\ wt\%\ SMER = \frac{SMER\ weight}{Whole\ weight} \times 100\%$$

To accelerate the curing of the SMER composite coating, the MEKP and 593 epoxy resin curing agent were stirred at a 1:1 feed ratio for 10 min to prepare a novel curing agent. Methyl ethyl ketone peroxide can initiate copolymerization reactions between vinyl resins and carbon-carbon double bonds, forming a three-dimensional network.

Then, the curing agent was incorporated into the aforementioned solution and stirred at 25 ℃ for 20 min, and SMER composite coating solutions were subsequently synthesized.

2.3 Spraying process for combustible cartridge case

The aforementioned SMER composite coating solutions were stirred for 10 min for future utilization. According to previous coating methods [42-43], the initial mass of all components was measured using a high-precision analytical balance, and then the coating concoction was thoroughly stirred for 3–5 min to guarantee proper mixing. The coating blend was uniformly applied to the CBT substrate surface using an electric spraying apparatus (SG0140-EU650) coupled with an electrostatic-assisted coaxial atomization nozzle (outer capillary inner diameter of 2.0 mm and inner capillary inner diameter of 0.8 mm), with the CBT specimen dimensions being 30.0 × 10.0 × 0.25 cm. Prior to coating, all specimens were pre-cleaned with absolute ethanol. During the spraying process, the core and shell feed flow rates were maintained at 0.5 mL/h and 1.0 mL/h, respectively, at an applied voltage of 9 kV and a nozzle-to-substrate spraying distance of 20 cm. Afterward, the coated CBT samples were air-dried and cured at 25 °C for 48 h. Ultimately, the cured coated CBT samples were subjected to saltwater-immersion/uptake, heat-resistance, WCA, and uniaxial tensile testing. To assess the correlation between the SMER concentration and protective roles of the SMER composite coating, we synthesized four types of mixture solutions according to the SMER content: 10 wt% SMER, 20 wt% SMER, 30 wt% SMER, and 40 wt% SMER. The detailed formulas of each coating are listed in Table 1.

2.4 Characterization

The cured CBT coatings were inspected using scanning electron microscopy (SEM, JEOL JSM-IT300, Tokyo, Japan) to visualize the surface texture and measure the scale of degradation. To inhibit surface charging, all samples were sputter-coated with gold for 60 s and examined at an accelerating voltage of 5 kV. Subsequently, the samples were observed across multiple magnifications (with scale bars of 5, 10, 50, and 200 μm, as well as 500 μm after saltwater immersion) to thoroughly appraise the general protective efficiency of the coatings. Energy-dispersive X-ray spectroscopy (EDS) attached to the SEM was utilized to map the spatial distributions and semi-quantitatively determine the surface elemental compositions of C, N, and Si via electron-beam-excited characteristic X-rays. FT-IR spectroscopy (Nicolet iS50, Thermo Fisher Scientific, Waltham, MA, USA) was conducted in the attenuated total reflectance (ATR) mode over the wavenumber range of 4000–500 cm^{-1} (32 scans, 4 cm^{-1} resolution) using a diamond crystal as the internal reflective element (IRE). Subsequently, the surface chemical states of the coated surfaces were analyzed by X-ray photoelectron spectroscopy (XPS; ESCALAB 250Xi, Thermo Scientific, Waltham, MA, USA). The XPS measurements utilized a monochromatic Al Kα X-ray source with a photon energy of 1486.7 eV (pass energy of 20 eV for high-resolution scans), and all binding energies were charge-referenced to the adventitious hydrocarbon C 1s peak (C–C/C–H) at 284.8 eV.

TGA was conducted with reference to ASTM E1131-08, and DSC was performed with reference to ASTM E793-06.

Thermogravimetric analysis (TGA) was carried out using a synchronous thermal analyzer (STA 449 F3 Jupiter, NETZSCH, Selb, Germany) equipped with an ultra-microbalance (MK2-MC5, Mettler Toledo, Greifensee, Switzerland) in a high-purity nitrogen atmosphere at a purge flow rate of 50 mL/min. Approximately 8.0–10.0 mg of cured coating specimen was placed in an open alumina (Al_2O_3) crucible (70 μL). Prior to sample testing, blank crucible runs were conducted under identical heating profiles for baseline subtraction to eliminate buoyancy and instrumental drift effects. The specimens were raised from 30 to 800 °C at a pace of 10 °C/min, followed by a constant temperature hold at 800 °C for 30 min. Each formulation was measured in triplicate (n = 3) to ensure thermal reproducibility. Furthermore, because the mass fraction of thermally stable inorganic fillers (Si_3N_4,

sepiolite, and yttria-stabilized zirconia, totaling 6.5 g per batch) varied across formulations, both the total residual mass (overall char yield) and the organic-phase-normalized char yield were evaluated to distinguish the intrinsic char-forming capability of the organic matrix from the inorganic filler contribution. The differential scanning calorimetry (DSC) of SMER composite coating was determined by a TA Q100 DSC instrument (TA Instruments, New Castle, DE, USA). The temperature was adjusted from 50 °C to 550 °C in a nitrogen environment (flow rate of 50 mL/min), with heating rate of 10 °C/min.

2.5 Saltwater-immersion/uptake test

The saltwater-immersion/uptake test of the coated CBT (CCC) samples employed the following method: First, prior to immersion, the specimens were pre-conditioned in a vacuum oven at 50 °C for 24 h to constant mass, cooled in a desiccator, and weighed using an analytical balance (±0.1 mg) to record the initial dry mass (m_0). Subsequently, all samples were completely submerged in 3.5 wt% NaCl (aq), consistent with the salinity of seawater (based on concentration of standard seawater), prepared from an appropriate amount of sodium chloride and deionized water, maintaining a constant liquid-volume-to-sample-surface-area ratio of 10 mL/cm^2. According to the literature [27–30], the test condition maintained the temperature at 26 °C for 3 days. After immersion, the specimens were removed from the solution, gently blotted with lint-free filter paper within 30 s to remove adherent surface droplets without squeezing the porous substrate, and immediately weighed to obtain the wet mass (m_t). The saltwater uptake (absorption rate, W_s, wt%) was calculated according to the formula: W_s (%) = [(m_t − m_0) / m_0] × 100%. For every sample, five independent specimen replicates (n = 5) were carried out and the mean value ± standard deviation was calculated as the final result.

2.6 Heat-resistance test

The heat-resistance test was conducted with reference to previous studies [28, 29], using the time to first visible fume as the endpoint at 250-280 °C. Five replicate trials were conducted for each sample, and the average time was calculated.

2.7 Water contact angle (WCA) test

Water contact angles were measured using 4 μL deionized-water droplets with reference to ASTM D7334-

08 at ambient conditions (25 ± 1 °C and 50 ± 5% relative humidity). Prior to measurement, the cured coated specimens were conditioned in a desiccator for 24 h to ensure a clean, dry, and macroscopically flat surface state. Each droplet was gently deposited onto the coating surface using a micro-syringe, and the static contact angle image was captured at a fixed equilibration time of 5 s after droplet deposition using a high-speed CCD camera. For each formulation, measurements were conducted at three randomly selected non-overlapping positions on each of three independent parallel specimens (n = 3, totaling 9 readings per group), and the results were reported as mean ± standard deviation. In addition, contact angle variation was monitored over a 60 s residence period to account for potential droplet spreading or penetration, with the coated samples exhibiting minimal angle decay (< 2.5°) during the observation window.

2.8 Uniaxial tensile test

Dumbbell-shaped coated CBT composite specimens (consisting of the porous CBT substrate integrated with the cured surface coating layer, rather than free-standing coating films, prepared identically to the uncoated CBT control to ensure direct structural comparability) were subjected to uniaxial tensile evaluations in accordance with ASTM D638 (Type IV specimen geometry) aiming at understanding the mechanical attributes of the composite coatings enhanced with organosilicon. The specimens featured a gauge length of 25.0 mm, a narrow-section width of 6.0 mm, and an average total thickness of 2.60 ± 0.05 mm (comprising the 2.50 mm CBT substrate and ~0.10 mm cured coating layer), measured at three points along the gauge section using a digital micrometer. The nominal cross-sectional area was defined as the initial width multiplied by the total composite thickness ($A_0 = w \times t$) in the gauge region. By utilizing the MT 3017 Tensile and Brinell Testing apparatus at a constant crosshead speed of 5.0 mm/min under ambient laboratory conditions (25 ± 2 °C, 50 ± 5% relative humidity), each sample group was tested across five independent specimens (n = 5) to obtain reliable results.

3. Results and discussion

3.1 FT-IR and XPS analysis

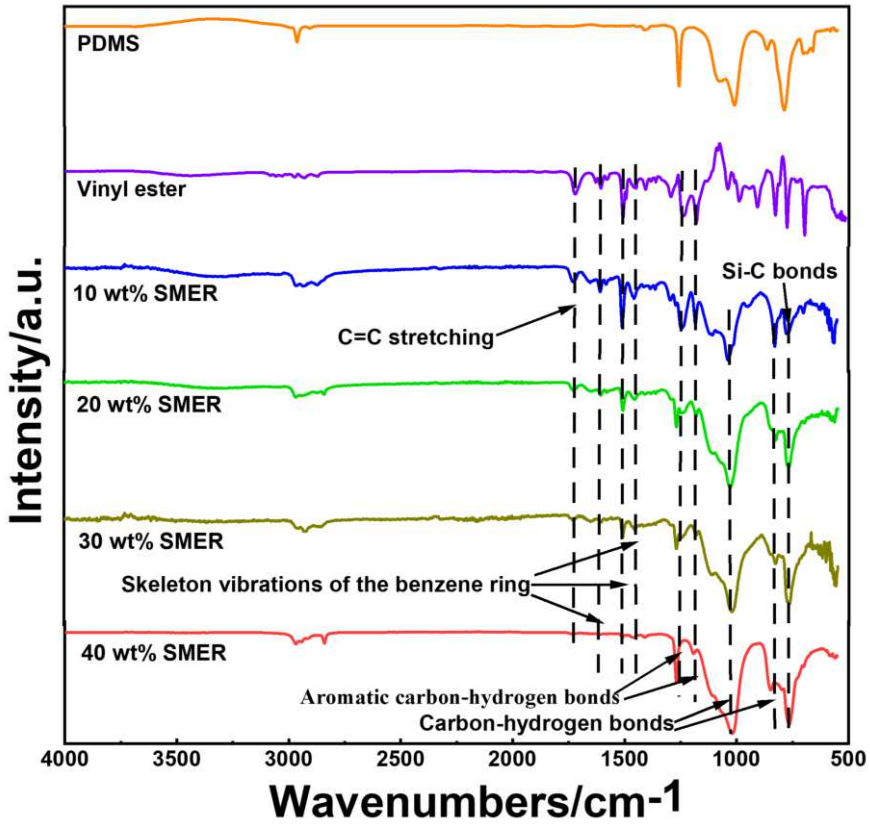


Fig. 4 FT-IR spectra of PDMS, VE, and SMER composite coatings containing 10, 20, 30, and 40 wt% SMER

Fig. 4 demonstrates the FT-IR spectra of the 10 wt% SMER, 20 wt% SMER, 30 wt% SMER, and 40 wt% SMER composite coatings. The absorption reaching a maximum at 1630 cm^{-1} corresponded to the C=C stretching of the esters in the vinyl ester resin. The maxima at 1450, 1510, and 1600 cm^{-1} belonged to the skeleton vibrations of the benzene ring [44]. Moreover, the maxima at 1194 and 1271 cm^{-1} corresponded to the bending vibrations of the C-H bonds in the vinyl groups, while the maxima at 1026 and 850 cm^{-1} were attributed to the aromatic carbon-hydrogen bonds (in vinyl ester) and ethylene double bonds, respectively [45-46]. The absorption peak at 774 cm^{-1} was ascribed to the Si-C bonds of the hydrocarbon groups attached to the silicon atoms [47].

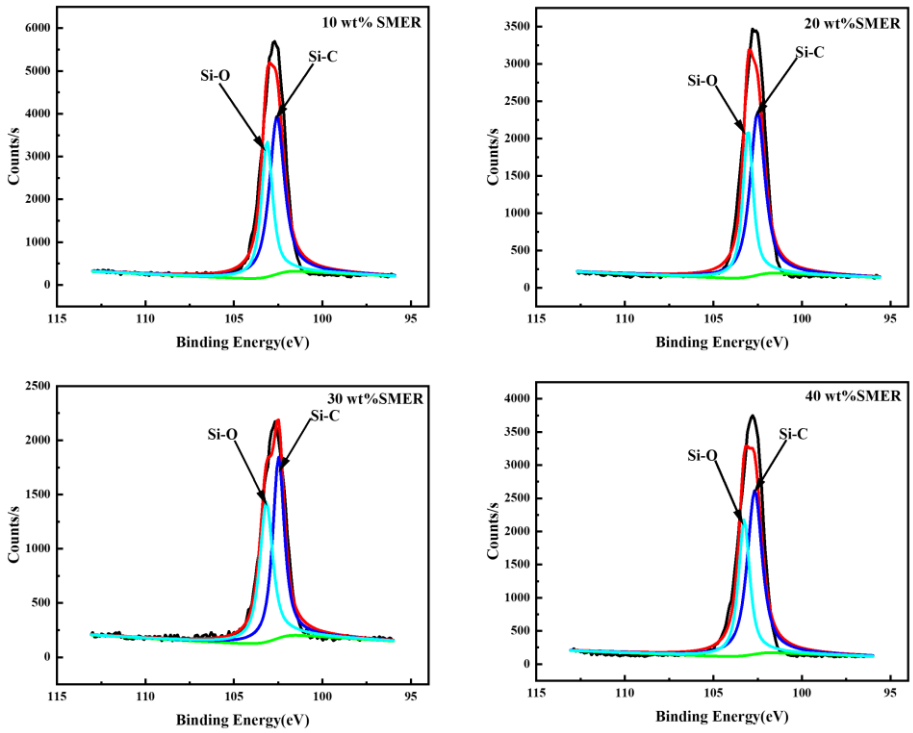


Fig. 5 High-resolution Si 2p XPS spectra and fitted components for (a) 10 wt%, (b) 20 wt%, (c) 30 wt%, and (d) 40 wt% SMER composite coatings

XPS was used to examine the surface chemical states of the SMER composite coatings (Fig. 5). All spectra were charge-corrected by referencing the adventitious hydrocarbon C 1s component (C–C/C–H) to 284.8 eV [48–52]. As shown in the high-resolution Si 2p spectra (Fig. 5a–d), the Si 2p envelope of all four SMER composite coatings can be deconvoluted into two primary sub-peaks centered at binding energies of approximately 102.3–102.5 eV and 103.3–103.5 eV. In accordance with literature assignments and reference databases [53–55], the lower-binding-energy component (~102.4 eV) is attributed to Si–C linkages in the organosilicon/PDMS-grafted segments (with potential minor overlap from Si–N environments in the Si_3N_4 filler near 101.8–102.1 eV), whereas the higher-binding-energy component (~103.4 eV) corresponds to Si–O–Si bonds in the siloxane backbone and silicate phases. Consistent across the 10–40 wt% SMER formulations, the coexistence of the Si–C and Si–O components in the Si 2p spectra, corroborated by the Si–C stretching band at 774 cm^{-1} in the FT-IR spectra (Fig. 4), confirms the successful incorporation of siloxane segments into the cured VE-based composite coating network.

3.2 Morphology

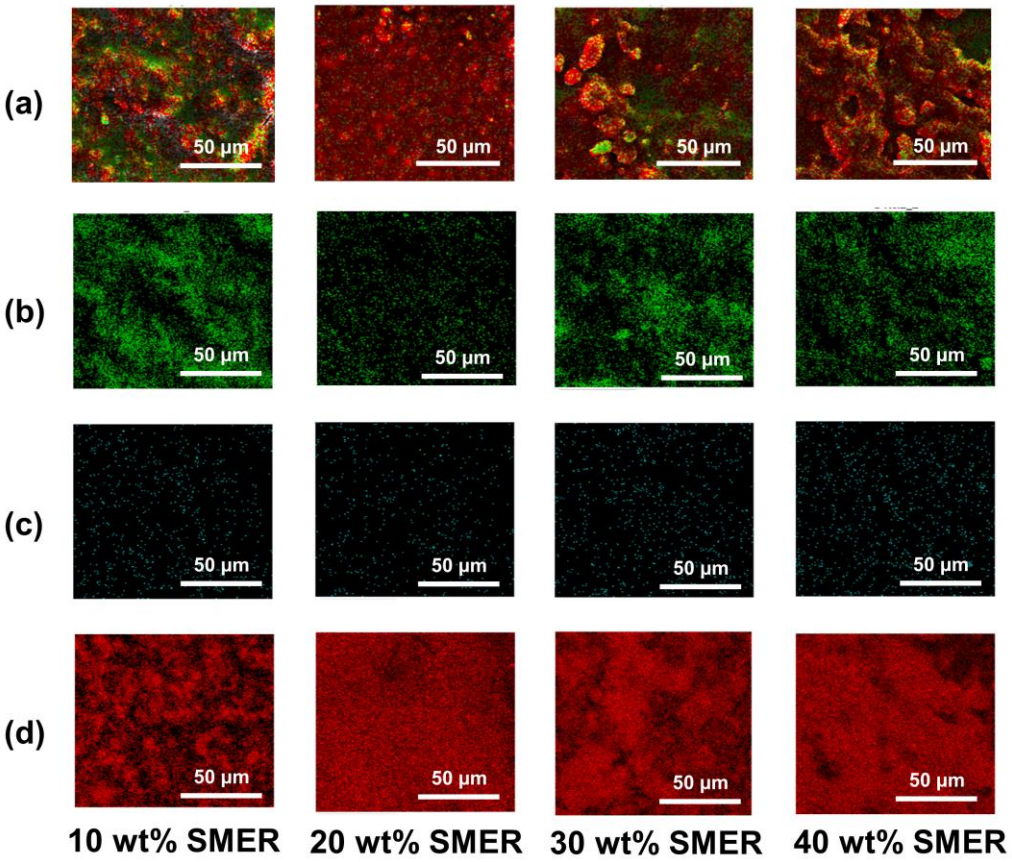


Fig. 6 SEM–EDS mapping images showing the distributions of C, N, and Si: (a) EDS element-distribution images of the SMER composite coatings, (b) carbon maps, (c) nitrogen maps, and (d) silicon maps

SEM images (Figs. 6 and 7) show that the coating morphology varies with SMER content. Local particle agglomeration and void-like features are visible in some samples, indicating that dispersion and coating compactness are composition dependent. The corresponding EDS maps provide qualitative information on the spatial distributions of C, N, and Si.

Table 2 Surface elemental concentrations of the SMER composite coatings

Sample	C (wt%)	N (wt%)	Si (wt%)
10 wt% SMER	83.23	2.36	0.53
20 wt% SMER	46.80	2.42	50.78
30 wt% SMER	75.63	1.86	22.51
40 wt% SMER	61.21	4.84	33.95

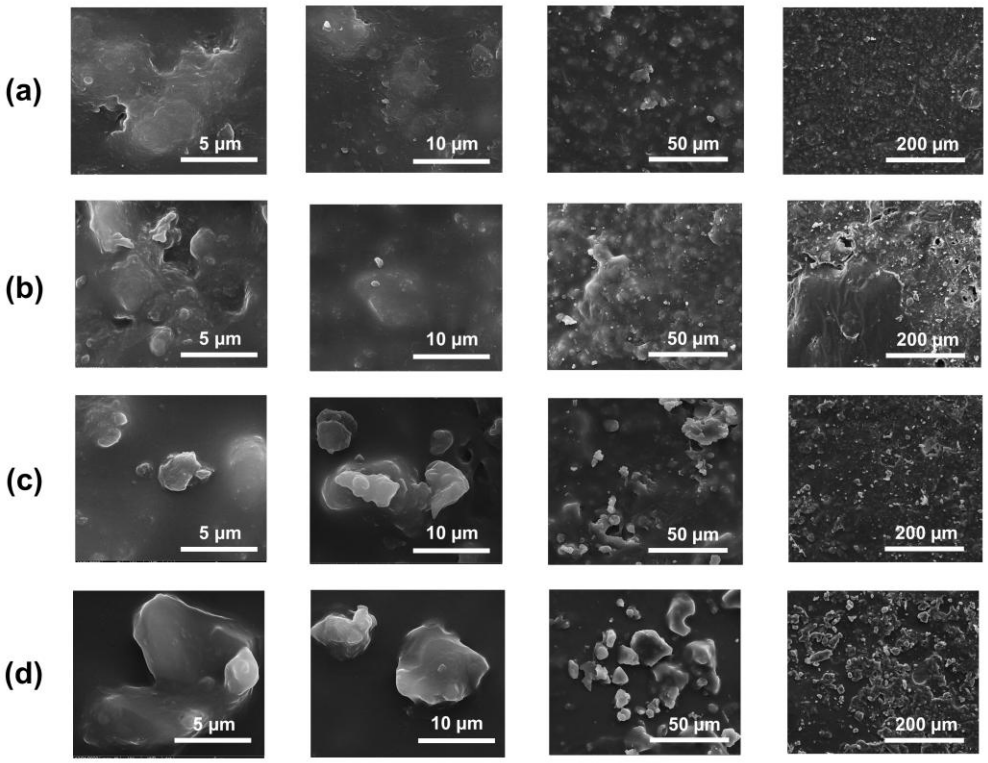


Fig. 7 SEM images of (a) 10 wt%, (b) 20 wt%, (c) 30 wt%, and (d) 40 wt% SMER composite coatings

The EDS results confirm the presence of C, N, and Si on the coated surfaces (Fig. 6 and Table 2), with substantial differences in the measured surface composition among the four formulations. These data support the incorporation of silicon-containing components but do not by themselves demonstrate specific Si-C or Si-O-Si bonds or prove formation of a cross-linked network; those chemical-state assignments should instead be based on the FTIR and properly fitted XPS results.

3.3 Thermal stability

The thermal behavior of the SMER composite coatings was evaluated by TGA/DTG under nitrogen. Representative curves for the 10, 20, 30, and 40 wt% SMER coatings are shown in Fig. 8a-d.

The TGA curves indicate multi-stage mass loss associated with removal of volatile species and subsequent degradation of the organic network. The low-temperature mass loss is plausibly related to absorbed moisture and/or residual low-molecular-weight components, whereas the principal degradation region reflects decomposition of the cured resin/siloxane network. The characteristic temperatures and char yields are summarized in Table 3.

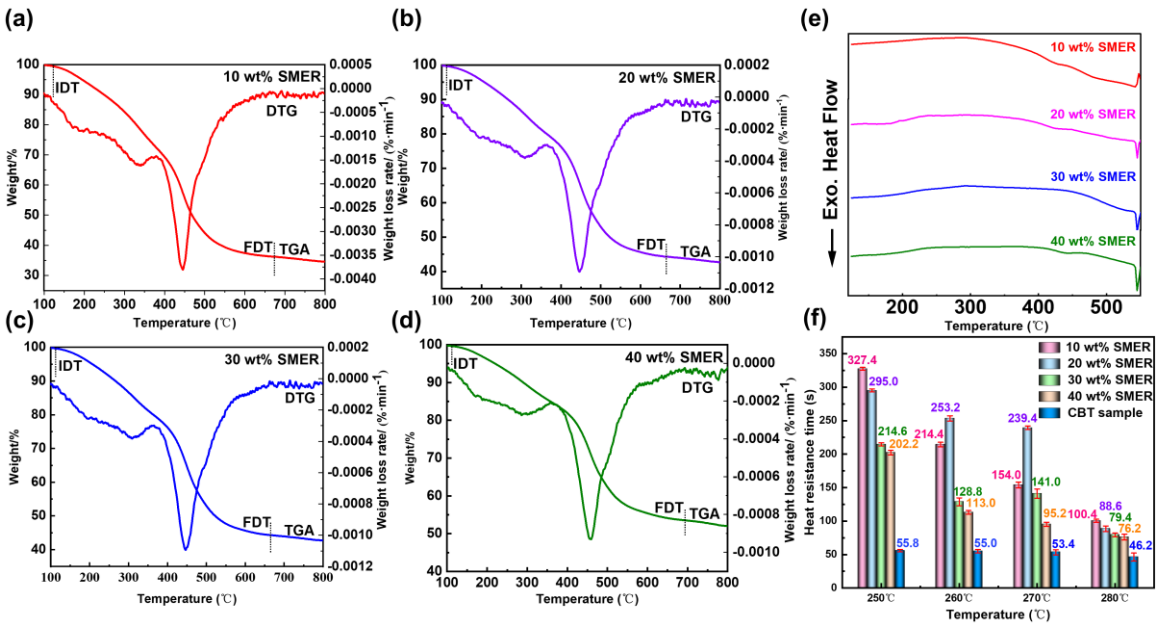


Fig. 8 (a–d) TGA and DTG curves for the SMER composite coatings, (e) DSC thermograms from the first heating run, and (f) average heat-resistance time of the coated CBT samples

Table 3 Thermal stability parameters of the SMER composite coatings obtained from TGA

Composite coating sample	IDT (initial decomposition temperature) (°C)	FDT (final decomposition temperature) (°C)	Temperatures (°C) at weight loss (%)			Char yield (%) at 700 °C
			5%	10%	20%	
10 wt% SMER	115	600	194	248	329	35.91
20 wt% SMER	119	620	207	266	363	43.94
30 wt% SMER	120	630	247	301	398	47.00
40 wt% SMER	122	642	219	290	417	53.46

Table 3 shows that the reported FDT increased from 600 °C for 10 wt% SMER to 642 °C for 40 wt% SMER, and the char yield at 700 °C increased from 35.91% to 53.46%. However, the temperatures corresponding to 5% and 10% mass loss did not increase monotonically with SMER content: the 30 wt% sample showed the highest $T_{5\%}$ and $T_{10\%}$, whereas the 40 wt% sample showed the highest $T_{20\%}$ and char yield. Notably, based on the formulation ratios in Table 1, the theoretical mass fraction of thermally stable inorganic fillers (6.5 g total) decreases from 29.28 wt% in the 10 wt% SMER coating to 26.00, 22.73, and 19.52 wt% in the 20, 30, and 40 wt% SMER coatings, respectively. After subtracting the theoretical inorganic filler fraction from the total residual mass at 700 °C, the net organic-derived char residue increases markedly from 6.63 wt% (10 wt% SMER) to 17.94, 24.27, and 33.94 wt% (20, 30, and 40 wt% SMER), corresponding to organic-phase-normalized char yields of 9.38%, 24.24%, 31.41%, and 42.17%, respectively. Thus, increasing SMER content mainly improved the later-stage thermal residue/barrier stability and intrinsic char/ceramization conversion of the siloxane-modified organic matrix rather than uniformly delaying the onset of mass loss.

The DSC curves (Fig. 8e) show thermal events in the high-temperature region that broadly overlap the principal decomposition range observed by TGA/DTG. Taken together, the TGA/DTG and DSC results indicate that the coating composition influences both the onset and later stages of thermal degradation.

The heat-resistance time decreased as the test temperature increased (Fig. 8f). At 250 °C, the 10 wt% SMER coating produced the longest time to first visible fume (327.4 s). At 260-270 °C, the 20 wt% formulation showed the best overall heat-resistance response. The non-monotonic dependence on SMER content is consistent with the

SEM observations: increasing the siloxane-rich fraction can improve barrier properties, but excessive loading may also increase heterogeneity or agglomeration and reduce coating compactness. Therefore, the optimum SMER content depends on the temperature range and the balance between network formation and coating morphology.

3.4 Water properties of the SMER composite coatings

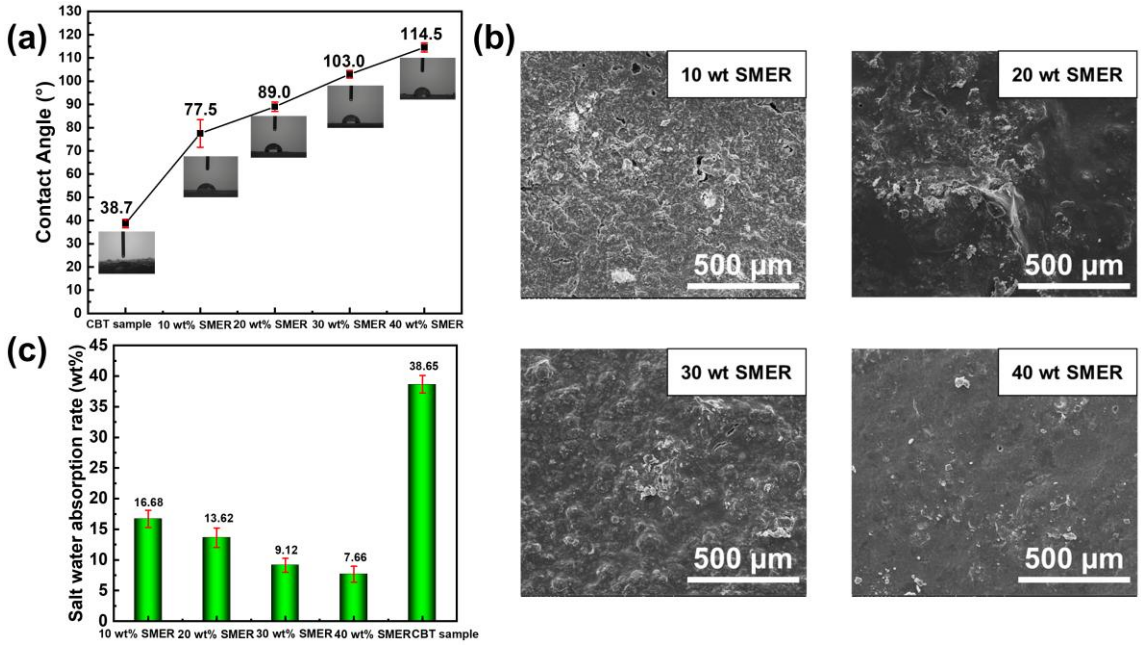


Fig. 9 (a) Water contact angles of the SMER composite coatings, (b) SEM images of coated CBT samples after immersion in 3.5 wt% NaCl solution for 3 d, and (c) saltwater absorption after 3 d of immersion

As shown in Fig. 9a, the water contact angle (measured at 5 s after droplet deposition across three independent specimens, n = 3) increased with SMER content, rising from 38.7 ± 1.8° for the uncoated CBT to 77.5 ± 5.6°, 89.0 ± 1.8°, 103.0 ± 1.5°, and 114.5 ± 1.6° for the 10, 20, 30, and 40 wt% SMER coatings, respectively. The 30 wt% and 40 wt% SMER coatings exhibited contact angles above 90°, indicating hydrophobic surface behavior with negligible droplet decay (< 2.5°) over 60 s, whereas droplets on the porous uncoated CBT rapidly penetrated the substrate. This trend is consistent with increasing enrichment of low-surface-energy siloxane-containing species at the coating surface, although surface roughness and local aggregation may also contribute to the measured contact angle.

19

After 3 d of immersion in 3.5 wt% NaCl solution, the coated CBT surfaces showed fewer and less pronounced defects than the uncoated substrate (Fig. 9b). The results indicate that the coating reduces direct liquid access to the porous cellulose-based substrate; however, SEM morphology alone should be interpreted as qualitative evidence of barrier integrity rather than as a direct measure of corrosion resistance.

The uncoated CBT exhibited a saltwater absorption of 38.65 wt%, whereas all coated samples showed lower values (Fig. 9c). The 40 wt% SMER coating gave the lowest saltwater absorption, 7.66 wt%, demonstrating the strongest saltwater/moisture barrier performance among the tested formulations. These data support improved resistance to saline-water penetration but should not be described as electrochemical corrosion resistance because no corrosion-rate or electrochemical measurements were performed.

3.5 Mechanical performance

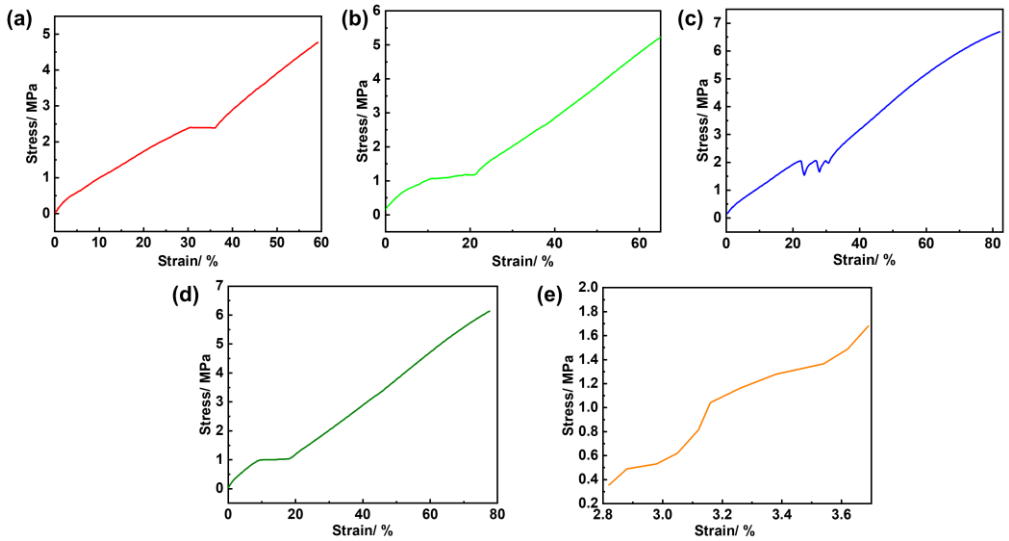


Fig. 10 Tensile curves for (a) 10 wt%, (b) 20 wt%, (c) 30 wt%, and (d) 40 wt% SMER composite coatings, and (e) the uncoated CBT sample

The coated CBT composite samples showed substantially higher elongation at break and engineering stress at break than the uncoated CBT (Fig. 10 and Table 4). The pronounced increase in elongation at break from 3.69 ± 0.29% for the brittle uncoated CBT to 59.19–82.06% for the coated CBT composites is attributed to the infiltration of the flexible organosilicon-modified resin into the surface pores of the cellulose fiber network, which bridges inter-fiber defects, suppresses premature crack initiation, and enables uniform load transfer across the

coated composite structure. Both parameters increased from 10 to 30 wt% SMER and then decreased at 40 wt%, indicating a composition-dependent optimum rather than a monotonic strengthening effect. The 30 wt% SMER coating exhibited the best tensile response among the coated samples, with an elongation at break of 82.06% and an engineering stress at break of 6.69 MPa. The reduction at 40 wt% is consistent with the greater morphological heterogeneity observed by SEM and suggests that excessive SMER loading can compromise effective stress transfer and coating uniformity.

Table 4 Tensile results of each sample

Coated sample	Elongation at break (%)	Engineering stress at break (MPa)
10 wt% SMER	59.19 ± 0.31	4.77 ± 0.03
20 wt% SMER	67.01 ± 0.31	5.41 ± 0.03
30 wt% SMER	82.06 ± 0.44	6.69 ± 0.02
40 wt% SMER	77.65 ± 0.61	6.14 ± 0.04
CBT sample	3.69 ± 0.29	1.68 ± 0.45

3.6 Mechanism analysis of the SMER composite coating

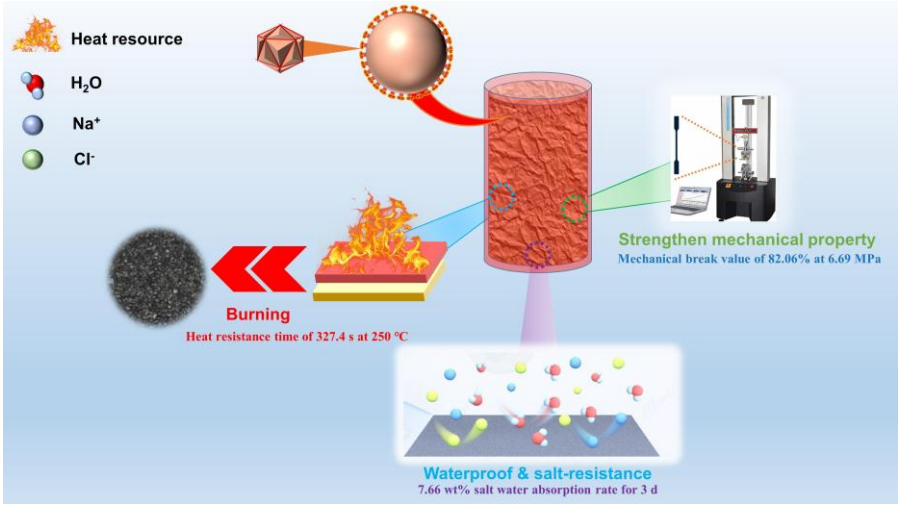


Fig. 11 Proposed mechanism of CBT protection by the SMER composite coating

Based on the combined characterization and performance data, the protective behavior of the SMER

21

coating is attributed to the interaction of the cured VE network, the siloxane-containing phase, and the inorganic fillers (Fig. 11). The aromatic VE backbone contributes rigidity and thermal resistance, while curing of the unsaturated groups forms a cross-linked organic network. Siloxane-containing segments reduce surface energy and improve water repellency, and the thermally stable inorganic fillers can increase the tortuosity of heat- and mass-transfer pathways. At the same time, the SEM results show that excessive SMER content can promote local heterogeneity or agglomeration, which helps explain why the heat-resistance and tensile properties do not improve monotonically with loading. The overall performance therefore arises from a balance among network formation, siloxane-rich surface chemistry, filler dispersion, and coating compactness rather than from a single proposed bond or reaction.

3.7 Comparison with previous studies

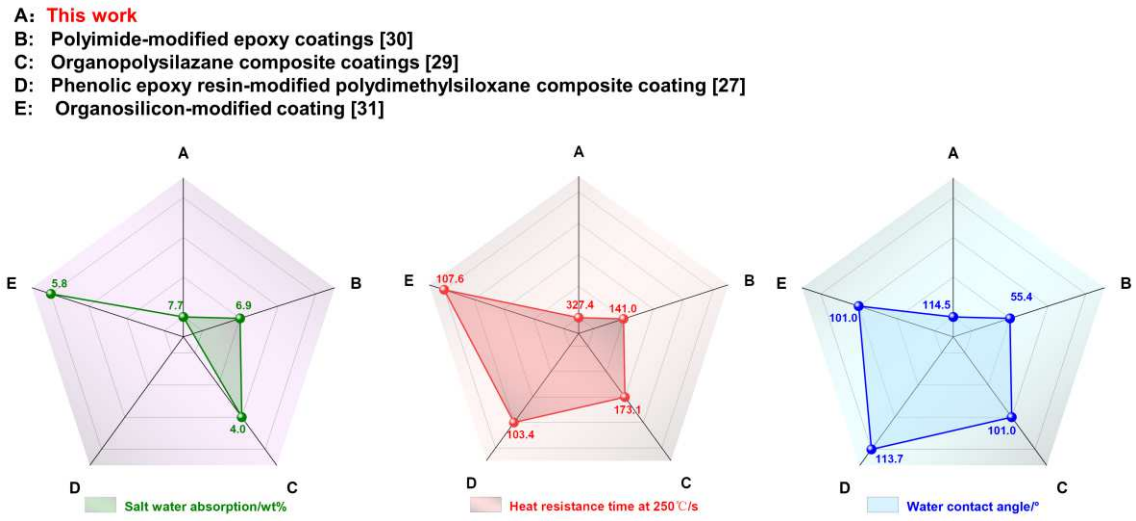


Fig. 12 Performance of the present coatings compared with previously reported systems

Increase in heat-resistance time (%) = [(t_coated − t_uncoated) / t_uncoated] × 100% = [(327.4 − 55.8) / 55.8] × 100% = 486.7%.

$$\frac{\text{Coated sample heat resistance time} - \text{CBT heat resistance time}}{\text{CBT heat resistance time}} \times 100\%$$

Figure 12 compares the performance of the present coatings with previously reported systems. Under the heat-resistance protocol used in this work, the 10 wt% SMER coating delayed the appearance of visible fume to

327.4 s at 250 °C, compared with 55.8 s for uncoated CBT. This corresponds to an increase of 486.7%, calculated using the uncoated CBT value as the baseline. After 3 d of immersion in 3.5 wt% NaCl solution, saltwater absorption decreased from 38.65 wt% for uncoated CBT to 16.68, 13.62, 9.12, and 7.66 wt% for the 10, 20, 30, and 40 wt% SMER coatings, respectively. These values represent reductions of 56.8%, 64.8%, 76.4%, and 80.2%, respectively, relative to uncoated CBT. The 40 wt% formulation therefore showed the lowest saltwater uptake among the tested coatings. The visual observations in Fig. 9b provide qualitative evidence of surface condition after immersion; numerical comparisons with literature should be limited to studies using sufficiently similar test conditions and endpoints.

4. Conclusions

SMER composite coatings improved the multifunctional protection of cellulose-based templates, but the results also show that no single SMER loading optimized every property. Increasing SMER content generally increased surface hydrophobicity and later-stage thermal residue stability: the 40 wt% coating reached a reported FDT of 642 °C, a char yield of 53.46% at 700 °C, and the lowest 3 d saltwater absorption of 7.66 wt%. In contrast, the 10 wt% coating gave the longest time to first visible fume at 250 °C (327.4 s), while the 30 wt% coating exhibited the best tensile response, with an engineering stress at break of 6.69 MPa and an elongation at break of 82.06%.

Statements and Declarations

Competing Interests

The authors declare no competing interests.

Data Availability

The data supporting the findings of this study are available from the corresponding author upon reasonable request.

Reproducibility Statement

The experimental procedures are described in the Materials and methods section, and the reported

measurements were obtained from replicate experiments as specified for each test.

References

[1] He S, Qian Y, Liu K, Macosko CW, Stein A (2018) Effects of inorganic fillers on toughening of vinyl ester resins by modified graphene oxide. Ind Eng Chem Res 57:4592–4599. https://doi.org/10.1021/acs.iecr.8b00362

[2] Pal N, Srivastava A, Agrawal S, Rai JSP (2005) Kinetics and mechanism of esterification of monoepoxies. Mater Manuf Process 20(2):317–327. https://doi.org/10.1081/AMP-200042132

[3] Jost N, Karger-Kocsis J (2002) On the curing of a vinylester-urethane hybrid resin. Polymer 43(4):1383–1389. https://doi.org/10.1016/S0032-3861(01)00702-9

[4] Buch X, Shanahan MER (2000) Thermal and thermooxidative ageing of an epoxy adhesive. Polym Degrad Stab 68(3):403–411. https://doi.org/10.1016/S0141-3910(00)00028-8

[5] Pakkanen ELK, Kainulainen TP, Heiskanen JP (2025) Furfural-based vinyl ester resins: syntheses, properties, and comparison to bisphenol A-glycidyl methacrylate-based vinyl ester resin. ACS Appl Polym Mater 7(15):10191–10200. https://doi.org/10.1021/acsapm.5c01980

[6] Sultania M, Yadaw SB, Rai JSP, Srivastava D (2010) Laminates based on vinyl ester resin and glass fabric: a study on the thermal, mechanical and morphological characteristics. Mater Sci Eng A 527:4560–4570. https://doi.org/10.1016/j.msea.2010.04.038

[7] Jaswal S, Thakur T, Gaur B, Singha AS (2022) High-performance gum rosin-modified hyperbranched vinyl ester resin derived from multifunctional pentaerythritol. Polym Bull 79:477–501. https://doi.org/10.1007/s00289-020-03511-x

[8] Gaur B, Rai JSP (1993) Rheological and thermal behaviour of vinyl ester resin. Eur Polym J 29(8):1149–1153. https://doi.org/10.1016/0014-3057(93)90324-9

[9] Siva P, Varma IK, Patel DM, Sinha TJM (1994) Effect of structure on property of vinyl ester resin. Bull Mater Sci 17(6):1095–1101. https://doi.org/10.1007/BF02757587

[10] Sultania M, Rai JSP, Srivastava D (2010) Studies on the synthesis and curing of epoxidized novolac vinyl ester resin from renewable resource material. Eur Polym J 46:2019–2032. https://doi.org/10.1016/j.eurpolymj.2010.07.014

[11] Rodriguez-Mella Y, López-Morán T, López-Quintela A, Lazzari M (2014) Durability of an industrial epoxy vinyl ester resin used for the fabrication of a contemporary art sculpture. Polym Degrad Stab 107:277–284. https://doi.org/10.1016/j.polymdegradstab.2014.02.008

[12] Mousa AA, Wagenknecht U, Gedan-Smolka M, Schneider A (2019) Cure characteristics and thermal behavior of organic–inorganic hybrid composite as assessed by DSC, TGA, and DMA techniques. J Sustain Metall 5(3):442–448. https://doi.org/10.1007/s40831-019-00234-w

[13] Agarwal S, Mishra A, Rai JSP (2003) Effect of diluents on the curing behavior of vinyl ester resin. J Appl Polym Sci 87(12):1948–1951. https://doi.org/10.1002/app.11543

[14] Li K, Wang K, Zhan M, Xu W (2013) The change of thermal-mechanical properties and chemical structure of ambient cured DGEBA/TEPA under accelerated thermo-oxidative aging. Polym Degrad Stab 98:2340–2346. https://doi.org/10.1016/j.polymdegradstab.2013.08.014

[15] Laot CM, Marand E, Oyama HT (1999) Spectroscopic characterization of molecular interdiffusion at a poly(vinyl pyrrolidone)/vinyl ester interface. Polymer 40:1095–1108. https://doi.org/10.1016/S0032-3861(98)80003-7

[16] Yang R, Wang Y, Ran X, Liu W (2023) A comparison study on toughening vinyl ester resins using different nanocarbon materials. Polymers 15:4536. https://doi.org/10.3390/polym15234536

[17] Zhang F, Zhao Y, Xu Y, Liu Y, Zhu P (2022) Flame retardation of vinyl ester resins and their glass fiber reinforced composites via liquid DOPO-containing 1-vinylimidazole salts. Compos Part B Eng 234:109697. https://doi.org/10.1016/j.compositesb.2022.109697

[18] Zhao Y, Chu Y, Xu Y, Zhu P, Wang Y (2023) Highly flame-retardant vinyl ester resins with well-balanced comprehensive performance. Chem Eng J 464:142659. https://doi.org/10.1016/j.cej.2023.142659

[19] Maaskant E, Tempelman K, Benes NE (2018) Hyper-cross-linked thin polydimethylsiloxane films. Eur Polym J 109:214–221. https://doi.org/10.1016/j.eurpolymj.2018.09.052

[20] Sia SK, Whitesides GM (2003) Microfluidic devices fabricated in poly(dimethylsiloxane) for biological studies. Electrophoresis 24(21):3563–3576. https://doi.org/10.1002/elps.200305584

[21] Esteves ACC, Brokken-Zijp J, Laven J, Huinink HP, Reuvers NJW, Van MP, With GD (2009) Influence of cross-linker concentration on the cross-linking of PDMS and the network structures formed. Polymer 50:3955–3966. https://doi.org/10.1016/j.polymer.2009.06.022

[22] Li W, Jing S, Wang S, Wang C, Xie X (2016) Experimental investigation of expanded graphite/phenolic resin composite bipolar plate. Int J Hydrogen Energy 41:16240–16246. https://doi.org/10.1016/j.ijhydene.2016.05.253

[23] Firpo G, Angeli E, Repetto L, Valbusa U (2015) Permeability thickness dependence of polydimethylsiloxane (PDMS) membranes. J Membr Sci 481:1–8. https://doi.org/10.1016/j.memsci.2014.12.043

[24] Zhang C, Zhang J, Xu T, Sima H, Hou J (2020) Effects of polyhedral oligomeric silsesquioxane (POSS) on thermal and mechanical properties of polysiloxane foam. Materials 13(20):4570. https://doi.org/10.3390/ma13204570

[25] Mo J, Ma W (2019) Silsesquioxane oligomer as replacement of polyhedral oligomeric silsesquioxane and its homo-blended polysilsesquioxane flexible thin film with low dielectric constant. Polym Sci Ser B 61(3):323–333. https://doi.org/10.1134/S1560090419030060

[26] Vandezande P, Gevers LEM, Vankelecom IFJ (2008) Solvent resistant nanofiltration: separating on a molecular level. Chem Soc Rev 37:365–405. https://doi.org/10.1039/B610848M

[27] Wu M, Xiao Z (2025) Enhancement of heat resistance and waterproof performance of combustible cartridge cases with phenolic epoxy resin-modified polydimethylsiloxane composite coating. Colloids Surf A Physicochem Eng Asp 708:136002. https://doi.org/10.1016/j.colsurfa.2024.136002

[28] Wu M, Xiao Z (2025) Fabrication of vinyl ester-modified phenolic resin composite coatings for the protection of combustible cartridge cases. ACS Omega 10(14):13807–13815. https://doi.org/10.1021/acsomega.4c06375

[29] Wu M, Xiao Z (2025) Optimum preparation of organopolysilazane composite coatings and their role in protecting combustible cartridge cases. Surf Interfaces 58:105804. https://doi.org/10.1016/j.surfin.2025.105804

[30] Wu M, Cao G, Xiao Z (2025) Polyimide-modified epoxy coatings reinforced with functional fillers for enhanced thermal stability and corrosion resistance. Adv Compos Hybrid Mater 8:172. https://doi.org/10.1007/s42114-025-01265-6

[31] Wu M, Du J, Xiao Z (2024) Preparation and properties of an organosilicon-modified coating to protect combustible cartridge cases. Colloids Surf A Physicochem Eng Asp 696:134380. https://doi.org/10.1016/j.colsurfa.2024.134380

[32] Aurtherson PB, Hemanandh J, Devarajan Y, Mishra R, Abraham BC (2022) Experimental testing and evaluation of coating on cables in container fire test facility. Nucl Eng Technol 54(5):1652–1656. https://doi.org/10.1016/j.net.2021.11.019

[33] Rukavina MJ, Skejić D, Milovanović B, Šćapec T (2024) Fire tests of load-bearing, light-steel-framed wall systems insulated with polyurethane foam. Appl Sci 14(2):637. https://doi.org/10.3390/app14020637

[34] Cancelliere P, Canzani P, Sassi S, Lucchini A, Messa S, Anselmi E (2021) A new test method to determine the fire behavior of façades with ETIC system. Fire Mater 45:624–637. https://doi.org/10.1002/fam.2886

[35] Park MJ, Alemayehu RW, Ju YK (2022) Fire resistance performance of steel–polymer prefabricated composite floors using standard fire tests. Polymers 14(7):1488. https://doi.org/10.3390/polym14071488

[36] Cheng S, Chen Z, Sheng D, Dong W, Cao R, Su Z, Wu M, Zhu X, Xie A, Mukherjee S, Li W (2025) Sustainable electromagnetic interference shielding materials from cellulose-grafted n-type polymers. Nat Commun 16:8608. https://doi.org/10.1038/s41467-025-63665-y

[37] Islamova RM, Dobrynin MV, Ivanov DM, Vlasov AV, Kaganova EV, Grigoryan GV, Kukushkin VYu (2016) Bis-nitrile and bis-dialkylcyanamide platinum(II) complexes as efficient catalysts for hydrosilylation cross-linking of siloxane polymers. Molecules 21(3):311. https://doi.org/10.3390/molecules21030311

[38] Hamada T, Nakanishi Y, Okada K, Ohshita J (2021) Crack- and shrinkage-free ethylene-bridged polysilsesquioxane film prepared by a hydrosilylation reaction. ACS Omega 6(12):8430–8437. https://doi.org/10.1021/acsomega.1c00183

[39] Ye Z, Chen X, Zhang L, Wang J, Chen H, Zhang X, Zhao W, Yuan Z (2026) In situ construction of multifunctional organosilicon/organic hybrid resin coatings on wood surfaces based on the PMHS Si–H click reaction. ACS Omega 11(30):45485–45493. https://doi.org/10.1021/acsomega.6c05204

[40] Meier D, Huch V, Kickelbick G (2021) Aryl-group substituted polysiloxanes with high-optical transmission, thermal stability, and refractive index. J Polym Sci 59(20):2265–2283. https://doi.org/10.1002/pol.20210316

[41] Ishak A, Sonnier R, Otazaghine B, Longuet C (2023) Silazanes, a novel flax fibers functionalization: effect on silicone-based composites. Compos Part A Appl Sci Manuf 166:107382. https://doi.org/10.1016/j.compositesa.2022.107382

[42] Xing C, Yi M, Shan X, Wang X, Zhao X (2020) Sintering behavior of a nanostructured thermal barrier coating deposited using electro-sprayed particles. J Am Ceram Soc 103:7267–7282. https://doi.org/10.1111/jace.17384

[43] Çanak TÇ, Ünsal C, Serhatlı E, Sarac AS (2017) Superhydrophobic fluorinated acylonitrile coatings via electrospraying. Prog Org Coat 105:342–352. https://doi.org/10.1016/j.porgcoat.2017.01.013

[44] Ziaee S, Palmese GR (1999) Effects of temperature on cure kinetics and mechanical properties of vinyl-ester resins. J Polym Sci Part B Polym Phys 37(7):725–744. https://doi.org/10.1002/(SICI)1099-0488(19990401)37:7<725::AID-POLB23>3.0.CO;2-E

[45] Cook WD, Simon GP, Burchill PJ, Lau M, Fitch TJ (1997) Curing kinetics and thermal properties of vinyl ester resins. J Appl Polym Sci 64(4):769–781. https://doi.org/10.1002/(SICI)1097-4628(19970425)64:4<769::AID-APP16>3.0.CO;2-P

[46] Brill RP, Palmese GR (2000) An investigation of vinyl-ester-styrene bulk copolymerization cure kinetics using Fourier transform infrared spectroscopy. J Appl Polym Sci 76(10):1572–1582. https://doi.org/10.1002/(SICI)1097-4628(20000606)76:10<1572::AID-APP12>3.0.CO;2-C

[47] Schiavon MA, Ciuffi KJ, Valéria I, Yoshida P (2007) Glasses in the SiOCN system produced by pyrolysis of polycyclic silazane/siloxane networks. J Non-Cryst Solids 353:2280–2288. https://doi.org/10.1016/j.jnoncrysol.2007.03.004

[48] Kim D, Dhand V, Rhee K, Park SJ (2015) Study on the effect of silanization and improvement in the tensile behavior of graphene-chitosan-composite. Polymers 7(3):527–551. https://doi.org/10.3390/polym7030527

[49] David L, Bernard S, Gervais C, Miele P, Singh G (2015) Facile synthesis and high rate capability of silicon carbonitride/boron nitride composite with a sheet-like morphology. J Phys Chem C 119:2783–2791. https://doi.org/10.1021/jp508075x

[50] Bhandavat R, Singh G (2012) Synthesis, characterization, and high-temperature stability of Si(B)CN-coated carbon nanotubes using a boron-modified poly(ureamethylvinyl)silazane chemistry. J Am Ceram Soc 95:1536–1543. https://doi.org/10.1111/j.1551-2916.2012.05079.x

[51] Gunes IS, Cao F, Jana SC (2008) Evaluation of nanoparticulate fillers for development of shape memory polyurethane nanocomposites. Polymer 49:2223–2234. https://doi.org/10.1016/j.polymer.2008.03.021

[52] Finster J, Heeg J, Llinkenberg ED (1990) Chemical and structural order in silicon oxynitrides by methods of surface physics. Prog Surf Sci 35:179–184. https://doi.org/10.1016/0079-6816(90)90038-L

[53] Park S, Huo J, Shin J, Heo KJ, Kalmoni JJ, Sathasivam S, Hwang GB, Carmalt CJ (2022) Production of an EP/PDMS/SA/AlZnO coated superhydrophobic surface through an aerosol-assisted chemical vapor deposition process. Langmuir 38(25):7825–7832. https://doi.org/10.1021/acs.langmuir.2c01060

[54] Rao L, Liu Y, Zhou H (2022) Significantly improved cell affinity of polydimethylsiloxane enabled by a surface-modified strategy with chemical coupling. J Mater Sci Mater Med 33:66. https://doi.org/10.1007/s10856-022-06690-3

[55] Lee AY, Powell CJ, Gorham JM, Morey A, Scott JHJ, Hanisch RJ (2024) Development of the NIST X-ray Photoelectron Spectroscopy (XPS) Database, Version 5. Data Sci J 23:45. https://doi.org/10.5334/dsj-2024-045